Acta Oceanol. Sin., 2023, Vol. 42, No. 5, P. 42–56
https://doi.org/10.1007/s13131-022-2024-2
http://www.aosocean.com
E-mail: ocean2@hyxb.org.cn

Quantitative morphometric analysis of a deep-water channel in the Taranaki Basin, New Zealand

Wei Wu[1], Guangxu Wang[1], Changsong Lin[2], Weiqing Liu[1]*, Quan Li[1, 3], Zhendong Feng[4], Shuyuan Ning[1]

[1] Institute of Resources and Environment, Henan Polytechnic University, Jiaozuo 454003, China

[2] School of Ocean Science, China University of Geosciences, Beijing 100083, China

[3] Institute of Exploration Technology, CNOOC International Ltd., Beijing 100028, China

[4] College of Safety Science and Engineering, Henan Polytechnic University, Jiaozuo 454003, China

Received 2 July 2020; accepted 12 April 2022

Abstract

The morphological changes of deep-water channels have an important influence on the distributions of channel sand reservoirs, so it is important to explore the morphological change process of deep-water channel for the exploration and development of deep-water oil and gas. Based on a typical sinuous Quaternary channel (Channel I) in the Taranaki Basin, New Zealand, a variety of seismic interpretation techniques were applied to quantitatively characterize the morphological characteristics of the Channel I, and the relationships between the quantitative parameters and the morphological changes of the Channel I, as well as the controlling factors affecting those morphological changes, were discussed. The results are as follows: (1) in the quantitative analysis, six parameters were selected: the channel depth, width, sinuosity, and aspect ratio (width/depth), the channel swing amplitude (λ) and the channel bend frequency (ω); (2) according to the quantitative morphological parameters of the channel (mainly including three parameters such as channel sinuosity, ω and λ), the Channel I was divided into three types: the low-sinuous channel (LSC), the high-sinuous channel (HSC), the moderate-sinuous channel (MSC). U-shaped channel cross-sections developed in the LSC, V-shaped channel cross-sections developed in the HSC, including inclined-V and symmetric-V cross-sections, and dish-shaped channel cross-sections developed in the MSC; (3) the morphological characteristics of the LSC and MSC were related to their widths and depths, while the morphology of the HSC was greatly affected by the channel width, a change in depth did not affect the HSC morphology; (4) the morphological changes of the Channel I were controlled mainly by the slope gradient, the restricted capacity of the channel and the differential in fluid properties.

Key words: Quaternary, deep-water channel, geometrical morphology, quantitative analysis, Taranaki Basin, New Zealand

Citation: Wu Wei, Wang Guangxu, Lin Changsong, Liu Weiqing, Li Quan, Feng Zhendong, Ning Shuyuan. 2023. Quantitative morphometric analysis of a deep-water channel in the Taranaki Basin, New Zealand. Acta Oceanologica Sinica, 42(5): 42–56, doi: 10.1007/s13131-022-2024-2

1 Introduction

Deep-water channels are an important part of deep-water sedimentary systems (Deptuck et al., 2007; McHargue et al., 2011; Zhao et al., 2018a), and have become popular research objects in the field of deep-water petroleum exploration (Mutti and Normark, 1987; Deptuck et al., 2003; Mayall et al., 2006; Posamentier, 2003; Janocko et al., 2013; Alpak et al., 2013; Xu et al., 2017; Malkowski et al., 2018; Lowe et al., 2019). Deep-water channels, which develop in continental slopes or abyssal plains, are driven by gravity flows, traction currents or other fluids, and exhibit a variety of external morphologies, can be used as sediment depocenters and as conduits for transporting terrigenous sediment to abyssal basins (Dott, 1963; Khripounoff et al., 2003; Pichevin et al., 2004; Wynn et al., 2007; Kolla, 2007; Biscara et al., 2011; Yao et al., 2018). Since the discovery of deep-water channel systems, many researchers have carried out various studies focusing on the morphological changes of deep-water channels (Reimchen et al., 2016; Zucker et al., 2017), their filling processes (Gee et al., 2007) and architectures (Tek et al., 2022), and the processes by which deep-water channels migrate and evolve (Deptuck et al., 2003; Labourdette, 2007).

Compared with estuarine channels, channels in bay areas, and continental channels, deep-water channels develop differently in certain ways. For example, deep-water channels are found mostly in deep water environments, while the other three types of channels are mostly found in shallow water or surface environments. Furthermore, the channels in bay areas have the same plane morphology as sinuous deep-water channels, but the causes of their sinuosity differ: the sinuosity of the former channel type is related mainly to the erosion degree of the fluid and the existence of slump blocks, which hinder the lateral migration of the channels and therefore affect the channel morphology (Gabet, 1998), while the sinuosity of the latter channel type is related mainly to factors such as the fluid properties and seafloor slope (Abreu et al., 2003; Mayall et al., 2006). Moreover, the plane morphology of both estuarine channels and deep-water chan-

Foundation item: The National Natural Science Foundation of China under contract Nos 42077410, 41872112 and 42002031; the Key Scientific Research Projects in University of Henan Province under contract No. 18A170007.
*Corresponding author, E-mail: weiqingliu@hpu.edu.cn

nels is changeable, but the development of estuarine channels is affected not only by natural factors but also by human activities: in contrast, human factors often have more intense and direct impacts on estuarine channels than on deep-water channels (Dai et al., 2013; Mei et al., 2018; Zhou et al., 2020). In other words, deep-water channels are generally not directly affected by human activities and are often influenced by natural factors (Gee and Gawthorpe, 2006). Therefore, regardless of the types of channel, its morphological changes are a major focus of research.

During the 21st century, with the rapid development of deep-sea exploration and geophysical technology, quantitative analyses of deep-water channels have become important yet difficult points of research (Hudson and Kesel, 2000; Gee et al., 2007; Straub et al., 2011; Gamboa and Alves, 2015; Qin et al., 2016; D' Alpaos et al., 2017). Babonneau et al. (2002) and Liu et al. (2012), along with other researchers, measured the quantitative geometrical parameters of deep-water channels, including their depth, width, and sinuosity. The effects of quantitative geometrical parameters on the morphological changes of the channels were subsequently analyzed (Niyazi et al., 2018).

The classification of the channel morphology has become a research hotspot. Accordingly, many studies have been conducted on this topic. According to the sinuosity of deep-water channels, their morphological types can be roughly divided into straight (Peakall et al., 2000; Gee et al., 2007), relatively straight (Reimchen et al., 2016), and either high sinuosity or low sinuosity (Clark et al., 1992; Clark and Pickering, 1996; Wynn et al., 2007; Babonneau et al., 2010; Harishidayat et al., 2015; Li et al., 2017b). In addition, scholars have proposed a variety of views on the definition of the sinuosity of different morphological channels. For instance, Clark and Pickering (1996) proposed that a sinuous channel is one whose sinuosity exceeds 1.50, whereas Wynn et al. (2007) suggested that the minimum sinuosity of a sinuous channel should be 1.20. In contrast, Reimchen et al. (2016) reported that the sinuosity of a relatively straight channel is 1.00–1.05, that of a low sinuosity channel is 1.05–1.20, and that of a high sinuosity channel is greater than 1.20. However, previous analyses of the morphological changes of channels focused too much on discussing the channel sinuosity and thus failed to comprehensively analyze the influences of various channel morphological parameters on their morphological changes.

Therefore, this study takes a Quaternary deep-water channel in the Taranaki Basin, New Zealand as the research object. Based on seismic interpretation techniques, various channel parameters are measured, the correlations between various parameters are comprehensively analyzed, and the morphological changes of the Channel I are explained. In addition, a quantitative analysis is performed to quantify the relationships between the morphological changes of the Channel I and their quantitative parameters and to finally explore the main factors controlling those morphological changes. This paper aims to develop approaches that are usable for employing seismic data to study the geomorphology of other basins elsewhere in the world.

2 Geological setting

New Zealand's Taranaki Basin has a complex tectonic history (Fig. 1). Its current tectonic morphology is related to the evolution of the Pacific-Australian plate boundary (Carter and Norris, 1976; Sutherland, 1999; King, 2000). Following its initial development in the Cretaceous, the basin evolved into a passive margin from the late Cretaceous to the Paleogene. The rapid and continuous supply of sediment from the eastern and southern uplifted hinterlands led to accumulation at the bottom of the basin and the formation of slopes (Masalimova et al., 2016). These sediments are known to be associated with volcaniclastic material originating from offshore volcanoes in the northern section of the basin, as well as the large-scale transport of sediment (King and Thrasher, 1996; Giba et al., 2013).

With the formation and development of the modern plate boundary, the proportion of clastic material is increasing. In addition, the Neogene was characterized by the uplift of the New Zealand landmass in response to compression across the plate boundary, which resulted in renewed erosion and the influx of large quantities of clastic sediments into most basins. Until the end of the Miocene, clastic sedimentation may have played a leading role in the development of large basin floor fans and channel systems (Uruski, 2008).

New Zealand's Taranaki Basin extends into the northwestern deep-sea area (Fig. 1a) and the basin area measures approximately 300 000 km^2 (Stagpoole et al., 2002). The basin is filled with Cretaceous to Quaternary sediment deposits (Fig. 1d), with some of the sediment exposed on the shores of the Taranaki Peninsula and the northernmost extent of the South Island. These areas are considered to be new exploration areas with an extremely low level of present exploration, as only a few shallow ocean drilling wells are currently located in the surrounding water. On a global scale, the Taranaki Basin is an ultra-deep-water frontier field and is considered to have major potential for deep-water oil and gas exploration and development in the future (Higgs et al., 2010). Relatively low-lying landform shoals, including the Lord Howe Uplift and Challenger Heights, are located west and southwest of the study area, while the West Norfolk Ridges are located east and northeast of the study area (Uruski, 2010; Li et al., 2017b) (Fig. 1a).

3 Database and methodology

3.1 *Seismic data*

We analyzed the publicly available Romney 3D seismic survey, which was acquired by Anadarko New Zealand between October 23 and December 6, 2011 and processed by ION Geophysical in February 2013 (NZP&M Petroleum Report available from www.nzpam.govt.nz) (Li et al., 2017b). The area of the 3D seismic data covering a depth of more than 1 000 m in the study area is approximately 1 700 km^2. The center of the study area is located at 38°00′45.22″S, 172°38′09.29″E. The time-migrated seismic data volume has a vertical sample interval of 4 ms and a horizontal bin size of 25 m×25 m. In addition, according to the spectrum analysis results, the dominant frequency in the shallow sediments is close to 35 Hz, and the seismic velocity in the seawater was determined to be approximately 1 600 m/s. The vertical resolution of the data is approximately 11 m, which successfully satisfies the requirements of this study (Li et al., 2017b).

3.2 *Methodology*

Based on the high-resolution three-dimensional (3D) seismic data collected in the study area, some seismic interpretation techniques, such as seismic cross-section analysis, seismic attribute extraction (e.g., variance and root mean square (RMS) amplitude) (Li et al., 2017a), and the combination of qualitative and quantitative analysis methods, were used to analyze the morphological characteristics of the channels.

During the research process, the top interface of the Quaternary was first tracked and interpreted using seismic interpretation

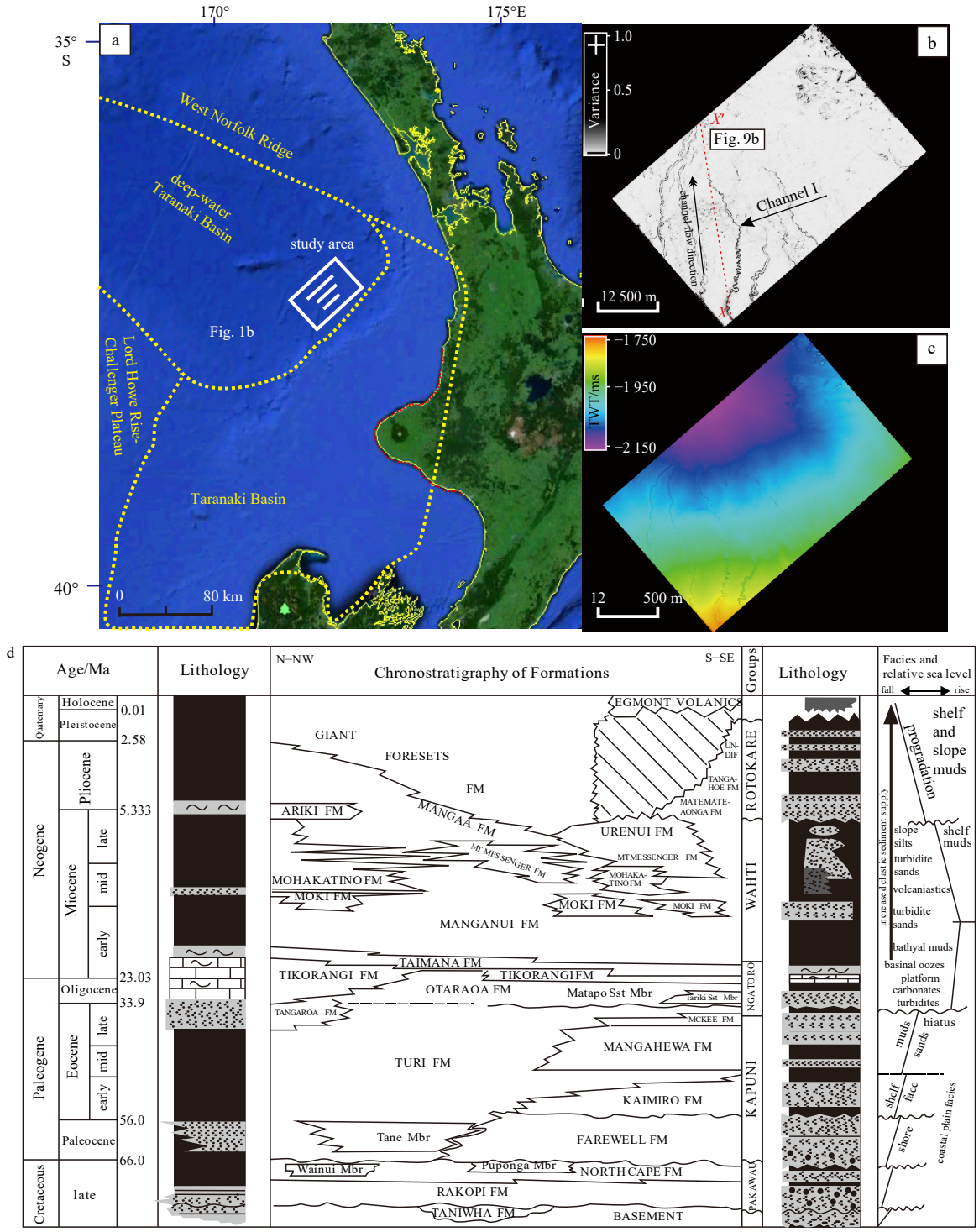

Fig. 1. Location maps of the study area. a. Deep-water Taranaki Basin situated in western New Zealand (after Li et al. (2017b)); the location of the 3D seismic study area is represented by the white rectangle. b. Variance map of the study area obtained from 3D seismic data that clearly shows the overall morphology of the Channel I. c. Bathymetric map of the area where the Channel I is located. d. Chronostratigraphy, generalized facies, and relative sea level relationships spanning the north–northwestern to south–southeastern regions of the Taranaki Basin (after Rotzien et al. (2014)). FM: formation.

software. The seismic variance attribute, which accurately reflects the morphological characteristics of submarine channels, was extracted to determine the external morphological characteristics of the Channel I. Then, based on the external morphology of the channel, the channel sinuosity was calculated as the ratio of the channel true length to the straight length (Fig. 2a), the amplitude of channel swing is defined as the vertical distance between the vertex of channel target bend and the straight line formed by the vertex of two adjacent bends.

In this study, 66 seismic cross-sections were obtained along

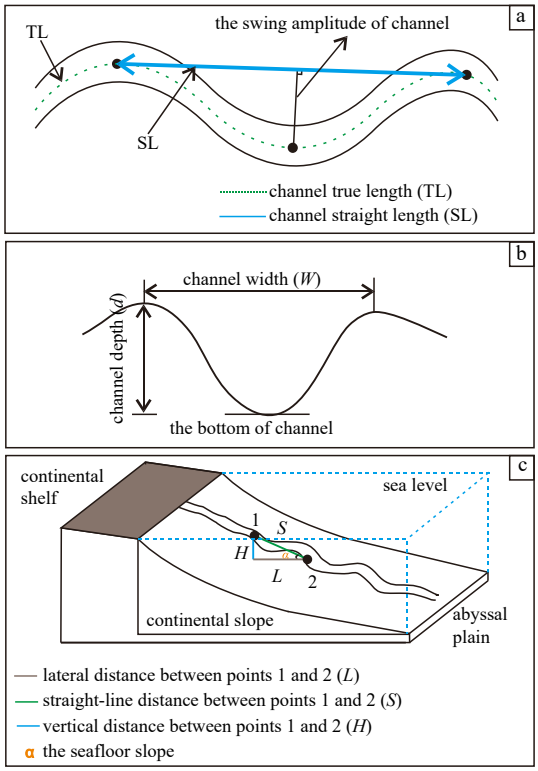

Fig. 2. Schematic drawing showing the methods adopted in this study to identify and measure the morphological parameters of the deep-water channel. a. Plan view showing the morphological parameters including the channel true length (TL), channel straight length (SL), and the swing amplitude of channel, in which the sinuosity was calculated as the ratio of the channel TL to the SL. b. Cross-sectional view showing the method adopted to measure the channel's width and depth. c. Stereogram showing the method used for measuring the slopes of the seafloor. α: seafloor slope gradient, in which the calculation formula of the seafloor slope gradient was as follows: α=arctan (H/L).

the Channel I from upstream to downstream. The shape of each seismic cross-section was identified based on the seismic reflection characteristics. The characteristics and types of the Channel I morphology were then analyzed. Based on the seismic cross-sections, various quantitative characteristic parameters of the deep-water channel were calculated. Regarding the measurements of the various quantitative characteristic parameters, the seismic cross-sections perpendicular to the provenance must be accurately interpreted under the constraints of the stratigraphy sections. First, the top and bottom interfaces (the top interface indicates the highest levee ridge position of the channel, the bottom interface indicates the deepest position at the bottom of the channel), and bilateral boundaries of the Channel I on the seismic cross-sections were determined (Zhao et al., 2018a; Li et al., 2019). Then, the distances between the left and right sides of the channel were measured to obtain the channel width (Niyazi et al., 2018) (Fig. 2b). The vertical distance between the top-bottom interfaces of the Channel I was calculated as the channel time depth (TWT), and a seismic velocity of 1 600 m/s was used to calculate the true depth (Fig. 2b). The seafloor slope gradient was defined as the ratio of the height differences of the channel sections to the straight-line distances of the channel sections, which were obtained by taking the arctan function of the values (Fig. 2c).

4 Results

4.1 *Characteristics of the quantitative parameters of the Channel I*

This research study conducted a quantitative analysis of a deep-water channel (Channel I) in the Taranaki Basin, New Zealand. The selected quantitative geometrical parameters included the channel width, depth, aspect ratio (width/depth), and sinuosity (Fig. 3).

It was found that in addition to large changes in sinuosity (Fig. 3b), there were also large differences in the channel width at various stages of channel development. The maximum channel width was determined to be 580.58 m, and the development position was mainly in the upper middle section; the minimum channel width was 37.37 m, and the development position was mainly in the lower section (Fig. 3d). Subsequently, these parameters were statistically classified to highlight the optimal value of each parameter (Fig. 4).

The sinuosity of the Channel I was further divided into three sections: 1.0 to 1.2, 1.2 to 1.5, and 1.5 to 4.0. The numbers of statistical samples were 9, 8, and 12, which accounted for 31.1%, 27.5% and 41.4%, respectively, of the total number of samples (Fig. 4a). The sinuosity of the Channel I was mainly high (1.5–4.0).

The width of the Channel I was divided into six sections: 0 m to 100 m, 100 m to 200 m, 200 m to 300 m, 300 m to 400 m, 400 m to 500 m, and greater than 500 m. The numbers of statistical samples were 3, 28, 20, 10, 3, and 2, and the percentages were determined to be 4.5%, 42.5%, 30.4%, 15.1%, 4.5%, and 3.0%, respectively. The main body of the Channel I was within 100 m to 400 m wide (Fig. 4b).

The depth of the Channel I was divided into four sections: 0 m to 10 m, 10 m to 20 m, 20 m to 30 m, and greater than 30 m. The numbers of statistical samples were 20, 28, 14, and 4, respectively, which accounted for 30.3%, 42.4%, 21.2%, and 6.1%, respectively, of the total number of samples (Fig. 4c).

The aspect ratio of the Channel I was divided into four sections as follows: 0 to 10, 10 to 20, 20 to 30, and greater than 30. The numbers of statistical samples were 10, 33, 12, and 11, and the corresponding percentages were 15.2%, 50.0%, 18.2%, and 16.6%, respectively (Fig. 4d).

4.2 *Plane geometrical morphology characteristics of the Channel I*

The Channel I in this study was oriented SE–NW overall. The seismic variance attribute of the Channel I was extracted to reflect the overall morphological characteristics of the Channel I (Fig. 5a). Various sinuous shapes of the Channel I were observed in the seismic variance attribute maps, with some channel sections displaying a relatively straight morphology. In addition, the sinuosity of the Channel I was measured, with the sinuosity ranging between 1.0 and 4.0. Previous studies classified channel types according to different ranges of channel sinuosity (Clark et al., 1992; Posamentier, 2003; Reimchen et al., 2016). In this study, in addition to referring to the channel sinuosity applied by our predecessors, we propose two other parameters, the channel bend frequency (ω) (the number of channel bends within the same distance) and the swing amplitude of channel (λ).

Combined with the measurement results of the quantitative channel parameters and the map of the plane morphology of the Channel I, the sinuosity of the Channel I was divided into three intervals, 1.0–1.2, 1.2–1.5 and 1.5–4.0 (Figs 3b and 4a). Then, the straight length of each channel section and the number of channel bends were measured in the three intervals (the number of bends counted by ω is not uniform with the previous statistical samples of the sinuous of the Channel I, because the sinuosity of

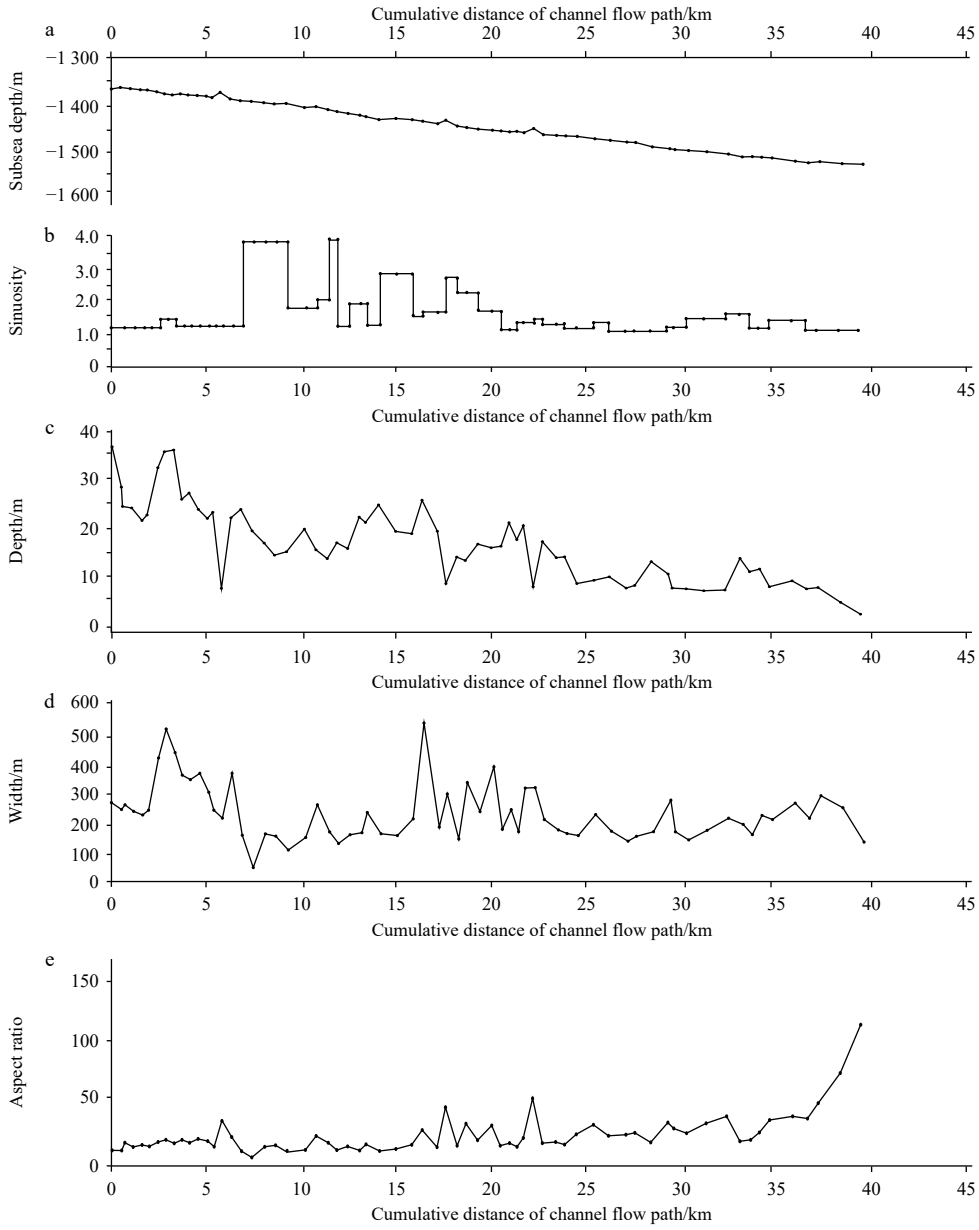

Fig. 3. Statistical analysis of the quantitative characteristic parameters of the Channel I in the study area. a. Subsea depth of the Channel I. b. Sinuosity of the Channel I. c. Depth of the Channel I. d. Width of the Channel I. e. Aspect ratio (width/depth) of the Channel I.

multiple bends in the Channel I is close to 1, so multiple bends are considered as a large bend when calculating the sinuosity), and ω was obtained. Within the channel sinuosity range from 1.0 to 1.2, the straight line distance of the channel was 5.7 km and the number of channel bends was 3 (Fig. 5b), so ω was 0.53; within the channel sinuosity range from 1.5 to 4.0, the straight line distance of the channel was 10.9 km and the number of channel bends was 24 (Fig. 5c), so ω was 2.20; and within the channel sinuosity range from 1.2 to 1.5, the straight line distance of the channel was 12.8 km, and the number of channel bends was 15 (Fig. 5d), so ω was 1.17.

Meanwhile, λ was measured (Fig. 5e). Within the channel sinuosity range from 1.0 to 1.2, the number of channel bends is small, and the swing amplitude varies little, with a maximum of 596.81 m, minimum of 395.72 m and average of 512.47 m. Within the channel sinuosity range from 1.5 to 4.0, the swing amplitude of the channel varies very much, with a maximum of 1 050.23 m, minimum of 296.10 m and average of 675.49 m. Within the channel sinuosity range from 1.2 to 1.5, the swing amplitude of the channel bends is basically consistent, with a maximum of 525.10 m, minimum of 357.00 m and average of 424.80 m.

The analysis result (Table 1) reveals that both sinuosity and ω show constantly increasing trends. With increasing sinuosity, *A*-*D*, *A*-*W* and *A*-λ show trends of first decreasing and then increasing. In contrast, the aspect ratio of the Channel I first increased and then decreased. Thus, sinuosity, ω and λ can be used as the main parameters to determine the morphology of the Channel I, while *A*-*D*, *A*-*W*, and the aspect ratio are auxiliary parameters.

Therefore, combined with sinuosity and ω, when the sinuosity of the channel is between 1.0 and 1.2, ω is less than 1.0, and λ varies little, the channel conforming to this condition can be defined as the low-sinuous channel (LSC) (Fig. 5b). Similarly, the

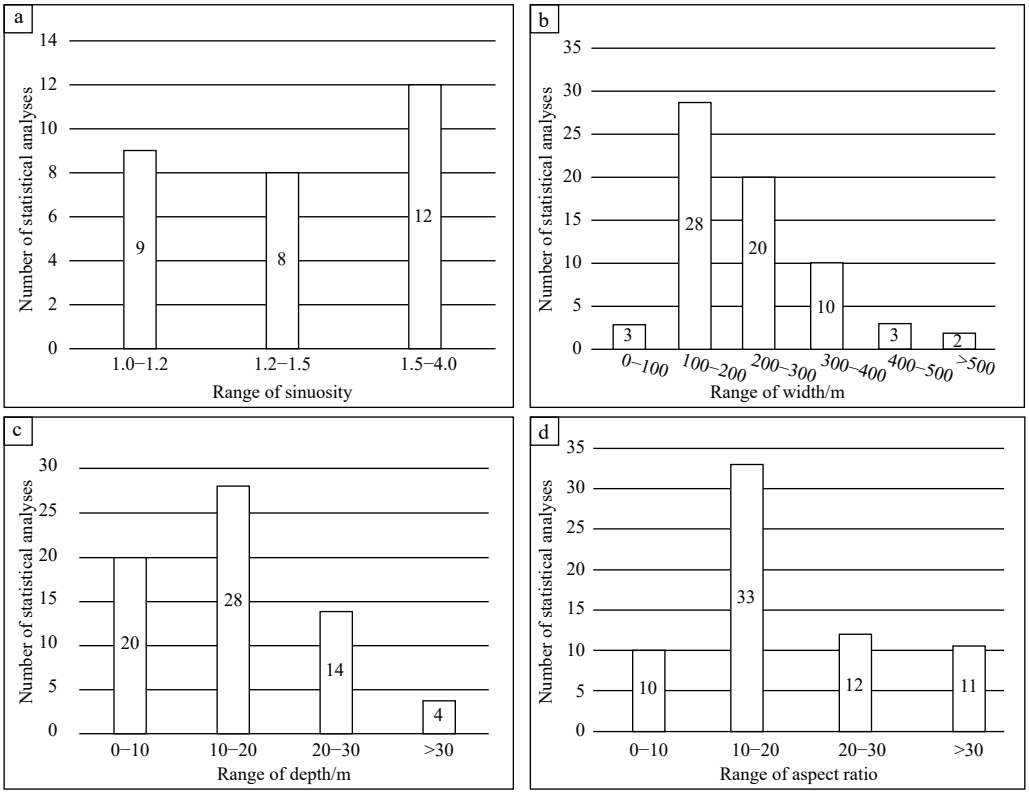

Fig. 4. Interval distributions of the quantitative characteristic parameters of the Channel I: statistical analyses of the sinuosity of the Channel I (a), width of the Channel I (b), depth of the Channel I (c), and aspect ratio (width/depth) of the Channel I (d).

channel with a sinuosity between 1.2 and 1.5, ω between 1.0 and 2.0 and λ tends to be consistent, can be defined as a moderate-sinuous channel (MSC) (Fig. 5c), and when the sinuosity of the channel is greater than 1.5, ω is greater than 2.0, and λ varies very much, the channel can be defined as a high-sinuous channel (HSC) (Fig. 5d). Moreover, in the plan view of the Channel I, the spatial distribution characteristics of the different channel morphologies are also shown. The LSC was mainly distributed in the upper section of the Channel I, while the HSC and MSC were located in the middle and lower sections of the Channel I (Fig. 5a).

4.3 *Geometrical characteristics of the Channel I on cross-sections*

The 66 seismic cross-sections demonstrated obvious spatial distribution characteristics (Fig. 6a) and change rules (referring to the changes in the cross-section geometrical morphology and the development of levees) (Fig. 7f). Therefore, 54 seismic cross-sections with easily identifiable shapes were selected, and their shape types were classified and summarized. In this study, based on the analysis results of the seismic cross-sections combined with previous research understanding (Deptuck et al., 2007; Zhao et al., 2018b; Yao et al., 2018), the channel cross-sectional geometrical morphology was divided into four types as follows: U-shaped (Fig. 6b), inclined V-shaped (Fig. 6c), symmetrical V-shaped (Fig. 6d), and dish-shaped (Fig. 6e).

Next, the number of samples and the spatial distribution of each cross-section type were determined (Fig. 7e). The number of U-shaped samples was 17, the number of inclined V-shaped samples was 22, the number of symmetrical V-shaped samples was 7, and the number of dish-shaped samples was 8. In the spatial distribution map of the deep-water channel cross-sections, strong spatial distribution characteristics were observed: the U-shaped cross-sections were mostly distributed in the upper reaches of the Channel I (Fig. 7a); the inclined V-shaped cross-sections were mostly in locations with high sinuosity with a wide distribution range and were distributed in the upper, middle and lower reaches of the Channel I (Fig. 7b); the symmetrical V-shaped cross-sections were mostly concentrated in the lower reaches of the Channel I (Fig. 7c); and the dish-shaped cross-sections were mostly distributed at the end of the Channel I (Fig. 7d).

In addition to the obvious spatial distribution characteristics, the different types of cross-sectional morphologies also exhibited certain change rules (Fig. 7f). Schematic diagrams of the cross-section morphologies and distributions of the Channel I are shown in Fig. 7f. A significant characteristic was discovered: the overall development of the Channel I from upstream to downstream changed from narrow and deep to wide and shallow.

The change rules of the Channel I cross-sections are clearly shown in the form of a table (Table 2). The locations where the U-shaped cross-section develops indicates a deep downcutting depth of the channel highly developed levee structures. The inclined V-shaped cross-sections mostly developed at the bends of the channel; as a result, the channel cross-sections of this type appear to be gentle on one side and steep on the other. At the locations of the channel where the symmetrical V-shaped cross-sections developed, the gradients on both walls of the channel are approximately equal and symmetrical, and the downcutting depths of the channel are relatively shallow compared to those of the former two cross-section types. The dish-shaped cross-sections are mostly distributed at the end of the channel with approximately the same width at the bottom and top of the channel; however, the downcutting depth of the channel is relatively shallow compared to those of the former three cross-section types, and the levees are not well developed.

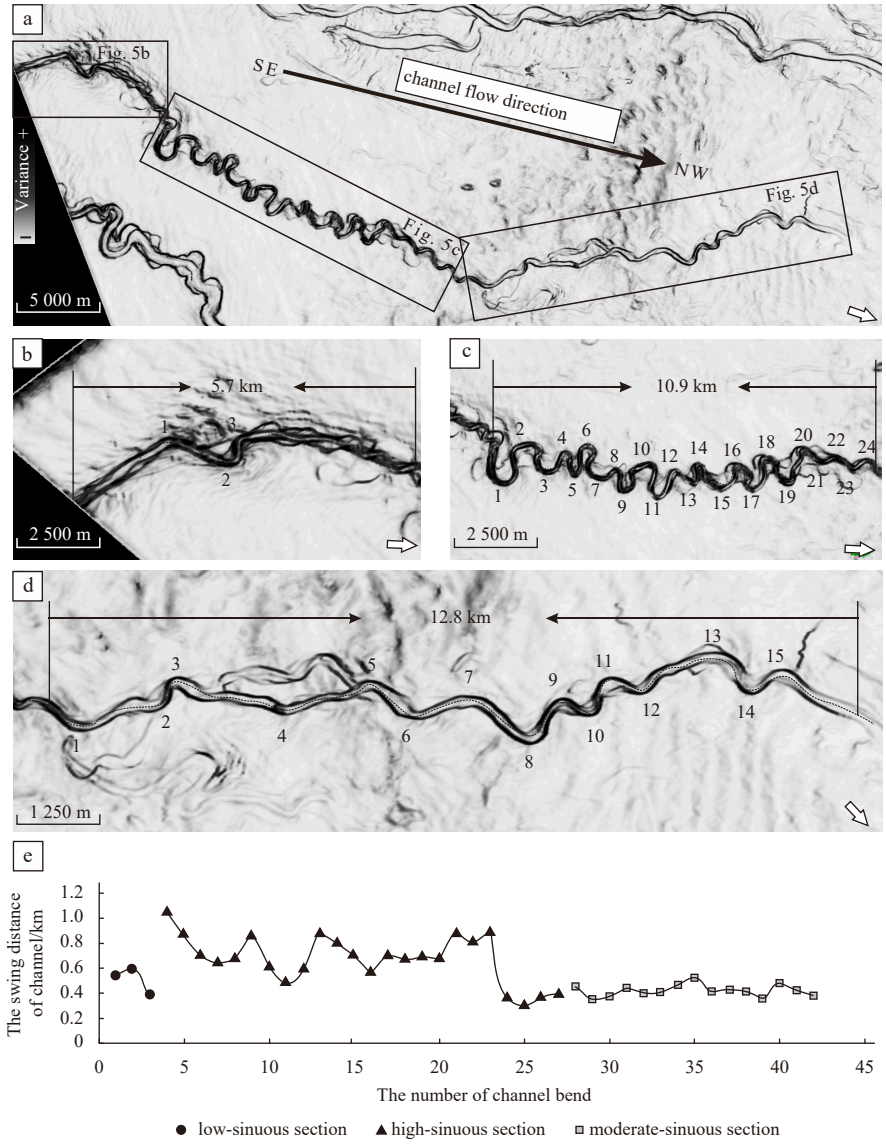

Fig. 5. Variance maps showing the different types of geometrical morphology of the Channel I in plan view. a. Overall morphology of the Channel I. b. Low-sinuous channel. c. High-sinuous channel. d. Moderate-sinuous channel. e. Variation in swing amplitude of channel bend. The box presents the different channel forms, and the numbers denote the bends of the Channel I.

Table 1. Quantitative parameters of the Channel I in different morphological sections

		LSC	MSC	HSC
Sinuosity		1.0–1.2	1.2–1.5	1.5–4.0
Width/m	Max-*W*	555.58	336.90	580.58
	Min-*W*	159.05	51.96	37.37
	A-*W*	323.77	196.12	215.43
Depth/m	Max-*D*	35.15	19.66	24.18
	Min-*D*	19.97	8.74	11.97
	A-*D*	25.33	13.23	16.48
Aspect ratio	Max-AR	35.43	110.16	43.22
	Min-AR	7.11	10.55	2.09
	A-AR	14.39	32.52	14.45
λ/m	Max-λ	596.81	525.10	1 050.23
	Min-λ	395.72	357.00	296.10
	A-λ	512.47	424.80	675.49
ω		0.53	1.17	2.20

Note: *A* is the average, AR is the aspect ratio, *W* is the width of the Channel I, *D* is the depth of the Channel I, ω is the channel bend frequency, and λ is the swing amplitude of Channel I. LSC: low-sinuous channel; MSC: moderate-sinuous channel; HSC: high-sinuous channel.

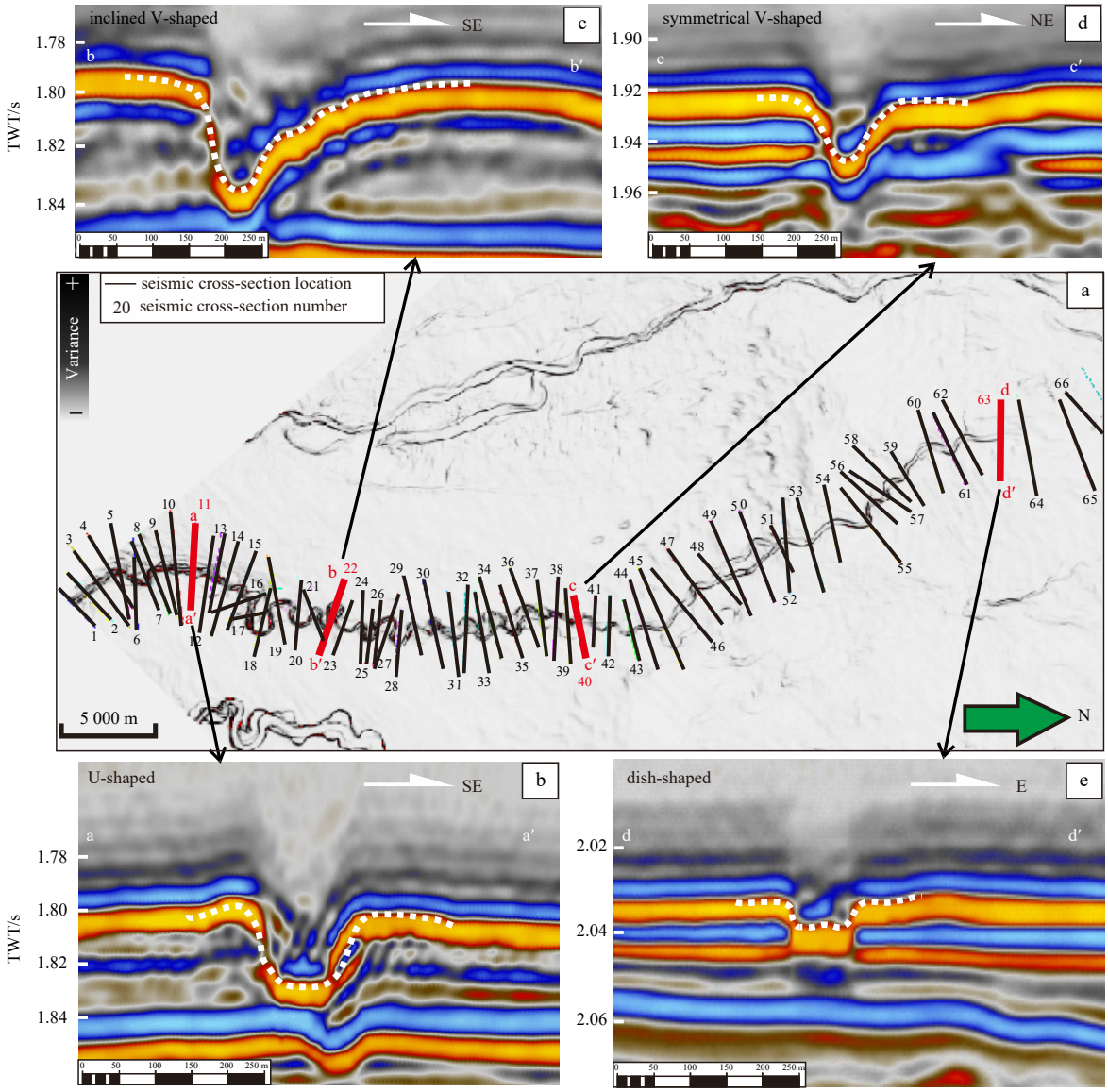

Fig. 6. Types of seismic cross-sectional morphologies of the Channel I. a. Locations of the seismic cross-sections are indicated by the solid black lines, the numbers are the channel cross-section labels, and the solid lines represent the various geometrical morphologies of the channel cross-sections: U-shaped (b), inclined V-shaped (c), symmetrical V-shaped (d), and dish-shaped (e).

5 Discussion

5.1 *Quantitative analysis of channel parameters*

The morphology of the Channel I varied during its evolution history. An important difference between a deep-water channel and an overland meandering river is that a deep-water channel is capable of self-regulation. Pirmez and Imran (2003) suggested that to achieve a smooth state in a deep-water channel, it is necessary to constantly adjust the sinuosity, gradient, depth, and width of the channel in response to changes in fluid flows and sediment loads. As a result, a certain rule was obtained by comparing the sinuosity of the channel with its width, depth, and other parameters, as detailed in Fig. 8. The relationships between these parameters can be used to quantitatively explain the causes of the changes in the Channel I morphology.

5.1.1 *LSC*

Figure 8a suggested that the correlation between the channel sinuosity and depth, while Fig. 8b indicated that the correlation between the channel sinuosity and width. In these two figures, the correlations between the sinuosity of the LSC and its width and depth are not significant. As observed from the above analysis, the sinuosity of the LSC varies in a small range from 1.0 to 1.2. However, Figs 8a and b suggested that the overall width and depth of the LSC are relatively large in the channel system (Table 1). At the same time, Fig. 8c suggested that a significant positive correlation between the depth and width of the channel, as the width of the channel increases with the depth.

5.1.2 *HSC*

For the HSC, there is no significant correlation between the sinuosity of the channel and its depth. The depth of the channel in this section is concentrated between 10 m and 25 m, the downcutting depth of the channel is 11.97 m at the shallowest and 24.18 m at its deepest, and its sinuosity range is 1.5–4.0 (Fig. 8a). The results suggested that regardless of how the sinuosity of the channel changes, the downcutting depth of the channel is concentrated only in the range between 10 m and 25 m, the change

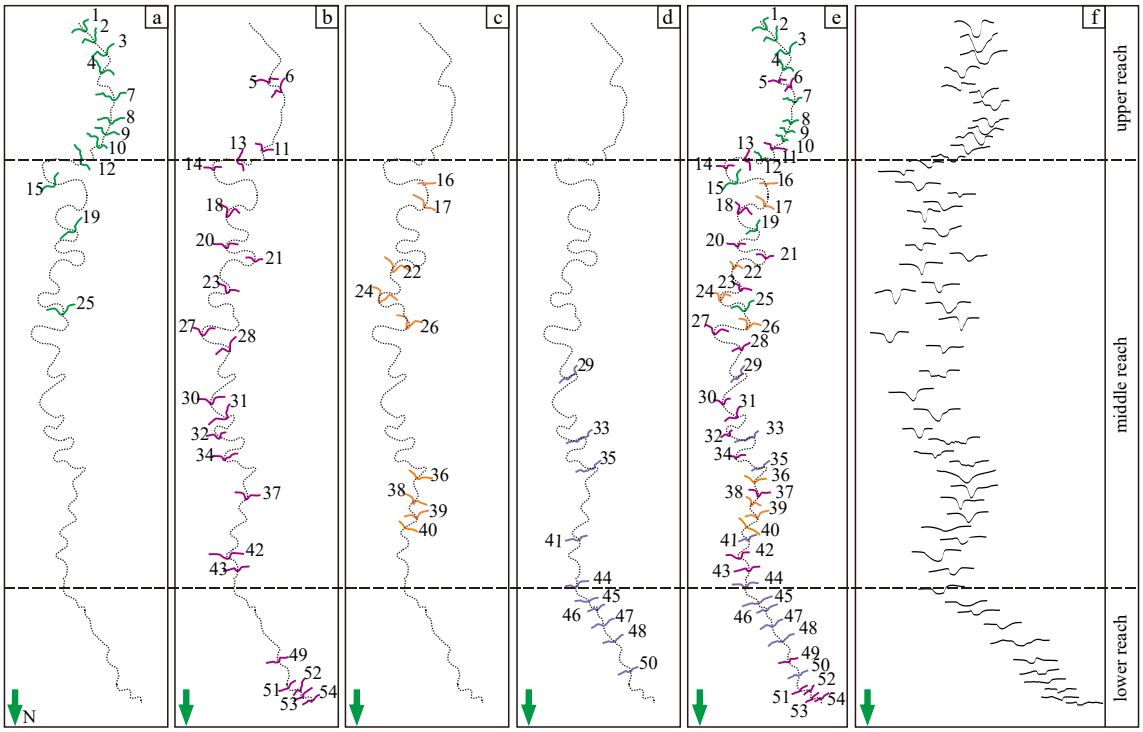

Fig. 7. Schematics of the spatial distributions of the different cross-sections of the Channel I. The specific location of four channel cross-sections geometrical morphology, such as U-shaped (a), inclined V-shaped (b), symmetrical V-shaped (c), and dish-shaped (d), in the whole Channel I. e. Spatial distributions of the overall channel cross-sections, where the numbers signify the sequence of the channel cross-sections. f. True morphology of each cross-section. From upstream to downstream, the depth of the Channel I gradually transitions from being narrow and deep to wide and shallow.

Table 2. Geometrical morphology characteristics of the Channel I on seismic cross-sections

Seismic facies	External geometries	Developed location	Characteristics	Seismic cross-section	Interpretation
a	U-shaped	middle and upper position of the channel	The gravity flow flowing through the channel has large scale, strong energy and strong undercut erosion ability. "Gull wing" levee structure is mostly developed in this area.	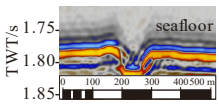	
b	inclined V-shaped	bend position of the channel	The scale of gravity flow decreases, the fluid energy decreases, and the undercutting erosion ability of the fluid is strong. Asymmetric levee structures are mostly developed in the channel in this area, and the concave bank slope of the levee is steep and the convex bank slope is slow.	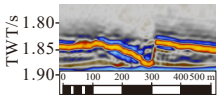	
c	symmetrical V-shaped	the straight section of the channel	The scale of gravity flow is small, the fluid has medium to weak energy intensity, and the undercut erosion ability of the fluid is weakened. Symmetrical V-shaped cross-sections are mostly developed in relatively straight channel sections.	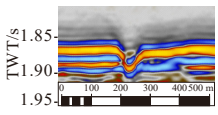	
d	dish-shaped	terminal position of the channel	The scale of gravity flow is very small and the fluid energy is weak. The channel is in a non-restrictive environment. The levee structure is basically undeveloped, and the bottom of the channel is relatively flat.	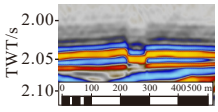	

of channel depth does not influence the sinuosity of the channel. Moreover, there is a significant negative correlation between the sinuosity of the channel and its width, as shown in Fig. 8b. The sinuosity of the channel decreases with increasing width, indicating that the sinuosity of the channel in this section is affected by changes in its width. At the same time, an analysis reveals no significant correlation between the width and depth of the channel in this section (Fig. 8d).

5.1.3 *MSC*

The MSC is similar to the LSC, there is no significant correlation between the sinuosity and either the width or the depth. In addition, the downcutting depth and width of the channel are relatively small in the channel (Figs 8a, b and Table 1). However,

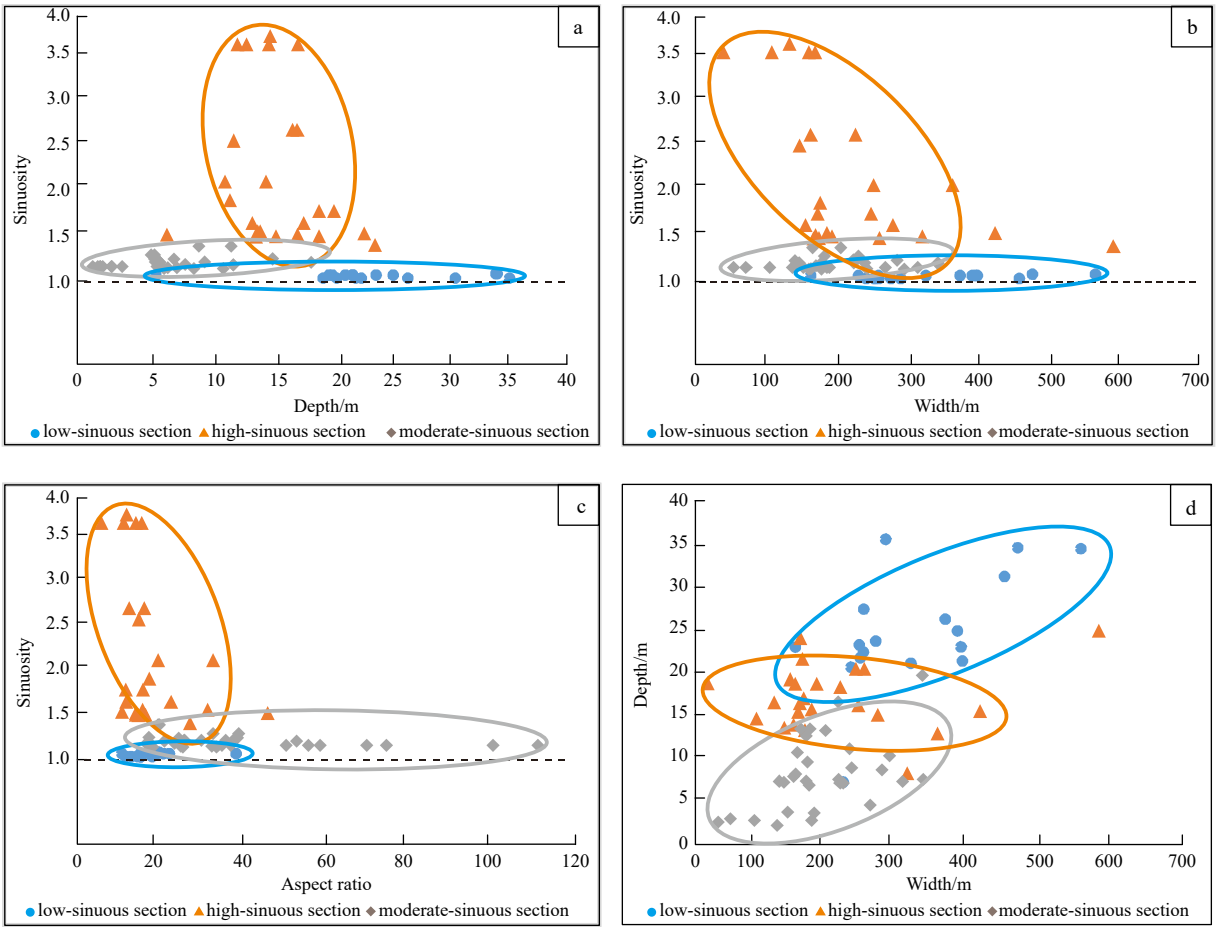

Fig. 8. Relationships between the quantitative parameters of the Channel I: relationships between the sinuosity and the depth (a), width (b), aspect ratio (width/depth) (c). d. Relationship between the width and depth of the Channel I.

Fig. 8d suggested that there is a significant positive correlation between the downcutting depth and width of the channel in this section, as the width of the channel increases with the downcutting depth.

5.2 *Why is the sinuosity of the middle reaches of the Channel I greater than that of the upper and lower reaches?*

In this study, a very interesting phenomenon is observed: the sinuosity of the middle reaches of the Channel I is much higher than that of the upper and lower reaches (Figs 3b and 5), which is different from the characteristics of the channels that developed in some other areas (Li et al., 2015). For instance, Li et al. (2015) analyzed the characteristics and sources of the deep-water channels in the Rio Muni Basin, West Africa, and suggested that the sinuosity of a submarine channel increases as the shelf gradient decreases, which is contrary to the characteristics of the Channel I described in this paper. Therefore, why is the sinuosity of the middle reaches of the Channel I of this paper greater than that of the upper and lower reaches?

The cause of the deep water channel's sinuosity remains disputed in the academic community. Generally, there are two types of mechanisms, the first is that the sediment inside the channel is jointly affected by lateral migration and downstream migration (Abreu et al., 2003), and the second is that the sediment in the channel moves laterally to the equilibrium profile and then swings back, resulting in the sinuosity of the channel (Peakall et al., 2000). Nevertheless, the sinuosity of a deep-water channel develops as a consequence of a dynamic and complex multistage process (Liu et al., 2012). In this study, due to the synchronicity and source consistency of the Channel I, the synchrony of internal factors such as sediment density in the channel is guaranteed to some extent, so the sinuosity of the deep-water channel should be affected by external factors such as the slope gradient, differences in fluid properties, and the restricted capacity of the channels.

5.2.1 *Slope gradient*

The Channel I in the study area was divided into three channel types, namely, the LSC (Fig. 5a), HSC (Fig. 5b), and MSC (Fig. 5c), in which the average slope gradients of the seafloor terrain were determined to be 3.91°, 3.31°, and 2.34° (Fig. 9). The calculation method is shown in Fig. 2c.

According to the measurements, the average seafloor slope gradient of the LSC is 3.91° (Fig. 9a). This section is located in the initial developmental region of the Channel I close to the source area, and receives a large amount of sediment from the continental shelf, so the fluid mass flowing inside the channel is large and energetic. Therefore, sediments erode the underlying strata along a relatively straight track, and the maximum downcutting depth was measured in the LSC (Fig. 3c).

From the LSC to the HSC, the average seafloor slope gradient decreases from 3.91° to 3.31° (Fig. 9a), with a large slope gradient variation range. In addition, fluid energy is gradually consumed during its flow along the channel. Therefore, in the HSC, the ca-

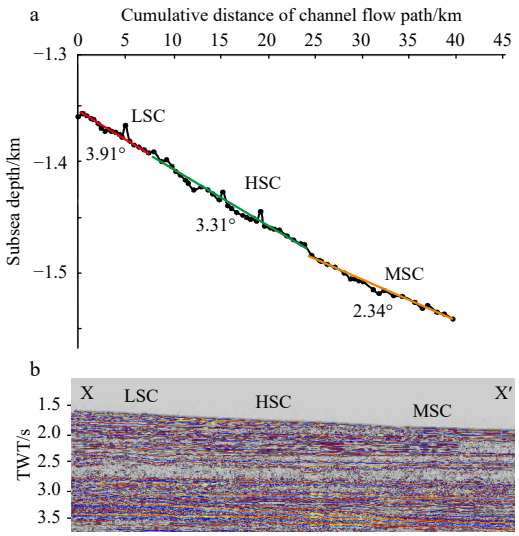

Fig. 9. Schematic diagram of the average seafloor slope gradient of the three sections of the Channel I. In a, the seafloor slope gradient of the low-sinuous channel (LSC) is 3.91°, that of the high-sinuous channel (HSC) is 3.31°, and that of the moderate-sinuous channel (MSC) is 2.34°.

pacity of the fluid in the channel to erode the underlying stratum is weakened, and the downcutting depth is correspondingly reduced (Fig. 3c).

From the HSC to the MSC, the average seafloor slope gradient decreases from 3.31° to 2.34° (Fig. 9a). A further decrease in the slope gradient leads to a slowdown in the flow rate of the fluid. This section is located at the end of the development of the Channel I, and thus, the fluid in this section of the channel has flown over a long distance. To overcome the friction between the fluid and the bottom of the channel, the energy consumption of the fluid is intense. Therefore, the erosion capacity of the fluid in this section of the channel is basically negligible; thus, the downcutting depth of this section is the shallowest among the channels (Fig. 3c), and this section is dominated mainly by accretion.

5.2.2 *Differences in fluid properties within the Channel I*

The sediment source-sink system has an important impact on the erosion and accretion of deep-water channels; the sediment in the source area may have been transported by rivers before entering the sink area (Dai et al., 2018). The source supply of the deep-water channel in the Taranaki Basin, New Zealand, is thought to have been derived from the northern part of the South Island and the western part of the North Island (Rotzien, 2013). The variations in the properties of the sediment in the source area lead to differences in the fluid properties inside the channel, which affects the erosion and accretion of the channel and controls the changes in the channel morphology.

With the continuous development of the Channel I, the properties of the fluid in the channel are constantly changing. In this study, due to the lack of core, drilling, and logging data, we can perform only an RMS amplitude attribute analysis of the 3D seismic data. Hence, combined with previous research experience, we conduct a simple analysis of the changes of the fluid properties within the Channel I to confirm that the differences in the fluid properties affect the morphology of the Channel I.

The LSC is located at the beginning of the whole channel system. According to the RMS amplitude attribute map, the axis of the channel in this section presents high amplitude reflections (Fig. 10), indicating that when a gravitational flow travels through this section, the sediment is coarse-grained and the proportion of debris flows in the channel is larger but the proportion of the turbidity currents is small; thus, this fluid has the strongest capacity to erode the underlying strata throughout the channel. The downcutting depth of the LSC was found to be the largest throughout the entire channel (Fig. 5c), and the width of the channel gradually increased with increasing downcutting depth (Figs 5d and 8d). Therefore, the sinuosity of the LSC remains basically unchanged, and the shape of the channel is controlled mainly by the width and depth, as is manifested in the transverse widening and vertical deepening of the channel; overall, the morphology of this channel type is approximately linear.

The Channel I develops from the LSC to the HSC, and the energy consumption of the fluid increases with an increase in the transport distance of the gravity flow. As seen from the RMS amplitude attribute map, from the upstream to the downstream re-

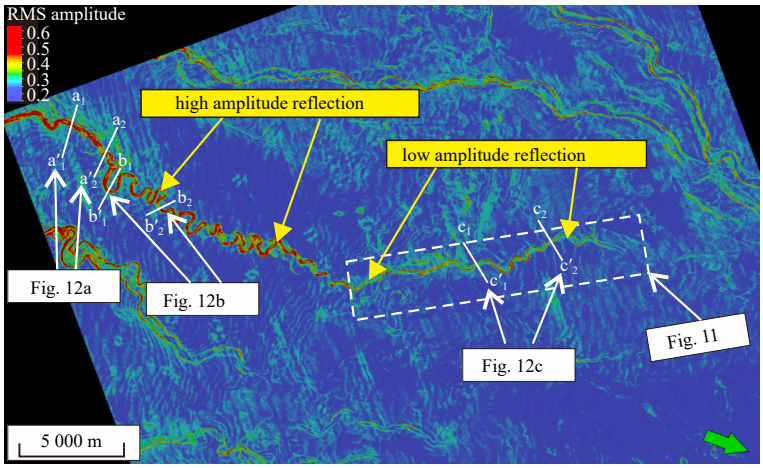

Fig. 10. Root mean square (RMS) amplitude attribute map of the Channel I. From upstream to downstream of the channel, the high amplitude reflections change to low amplitude reflections. In the low-sinuous channel and high-sinuous channel, the position of the axis of the channel is marked by high amplitude reflections, while in the moderate-sinuous channel, the axis of the channel is delineated by low amplitude reflections. The red and yellow positions indicate high amplitude reflections, and the green and blue positions indicate low amplitude reflections.

gion of the Channel I, the reflection amplitude of the axis of the channel changes from high to low (Fig. 10), indicating that the coarse sediment in the fluid is gradually deposited in the process of movement. In addition, the content of the debris flow decreases gradually while the turbidity current increases, weakening the downward erosion capacity of the gravitational flow to some extent. Due to changes in the seafloor slope gradient and fluid energy, the morphology of the channel gradually changes from straight to sinuous. The fluid erode and scour the concave bank wall of the channel, while the convex bank wall of the channel accretes through sediment deposition. This process repeats, resulting in the increasing sinuosity of the channel. When the sinuosity of the channel is increased to a certain extent, the capacity of the fluid to erode the concave bank wall is weakened, and thus, the channel no longer expands outwards. However, the sedimentation process of the convex bank wall continues, resulting in a gradual decrease in the width of the Channel I. Hence, the HSC adjusts the sinuosity of the channel mainly by altering the width of the channel so that the channel tends toward an equilibrium state.

The RMS amplitude map further shows that the MSC is dominated by low amplitude reflections, indicating that the energy of the gravitational flow fluid gradually weakens during long-distance transport, the main fluid in the channel manifests as a turbidity current, while the debris flow basically disappears (Fig. 10). Figure 8d shows that the downcutting depth of the channel continues to increase, indicating that the fluid at this stage still has a certain downcutting erosion capacity. According to Figs 11a and b, crevasses can be observed in the MSC. Nevertheless, the overall downcutting depth of the MSC is shallow (Fig. 3c), and the fluid tends to overflow the channel wall. When the fluid erodes the lateral wall of the channel, the sinuosity of the channel begins to increase. However, when the channel develops to a certain stage, it is easy for the fluid to break through the channel wall and break into a small crevasse channel. At this point, the ability of the fluid to erode the sidewall disappears, and the sinuosity of the channel also stops increasing. Therefore, the sinuosity of the channel in this section does not increase indefinitely; instead, after increasing to a certain extent, a crevasse forms within the channel, leading to the termination of the bending process of the channel. Thus, the channel currently presents a moderately sinuous external shape.

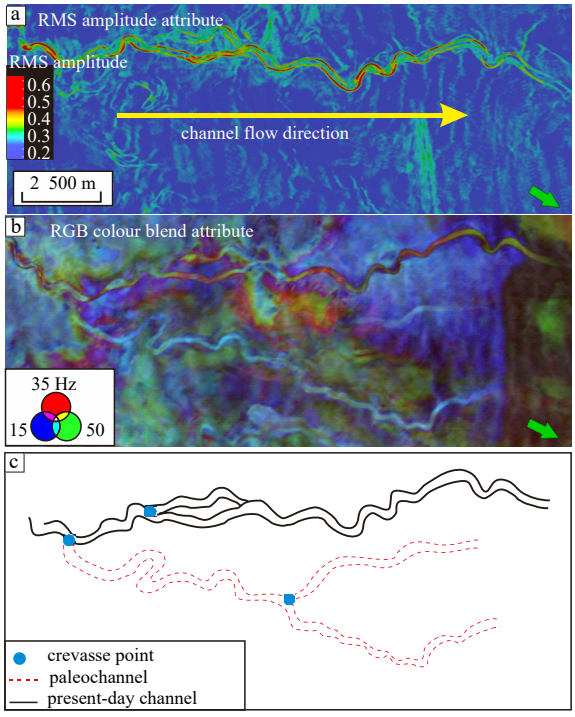

Fig. 11. Schematic diagram of a channel crevasse in the moderate-sinuous channel of the Channel I. a. Root mean square (RMS) amplitude attribute map. b. Red-Green-Blue (RGB) colour attribute map. c. Schematic illustration of the formation of a channel crevasse. The black curve represents the present-day channel, the red dotted line represents the paleochannel, and the blue circle represents the crevasse position. The specific location is shown in Fig. 10.

5.2.3 *The restricted capacity of the Channel I*

In addition to the influence of the seafloor slope gradient on the morphology of the channel, the restricted capacity of the channel also has a direct impact on the morphological change of the channel. Moreover, the restricted capacity is controlled primarily by the downcutting depth of the channel and the building capacity of the levees.

In the LSC, the sinuosity range is 1.0–1.2 (Fig. 3a). According to the results of the previous discussion on the slope, the LSC has the largest slope gradient (3.91°) (Fig. 9a) and the greatest overall downcutting depth (Fig. 3c). The greater the downcutting depth, the stronger the restricted capacity of the channel is. At the same time, the RMS amplitude attribute map and seismic cross-sections demonstrate that the levee structures in the LSC are highly developed (Figs 10 and 12a). The levees on both sides of the channel are overflow deposits formed by the fluid overflowing the channel, which also indirectly plays a role in restricting the lateral movement of the channel. The limiting effect of the maximum downcutting depth on the channel and the effect of the levees on the lateral movement of the channel caused the channel to be a strongly restricted environment, so the channel formed a low-sinuosity morphology.

For the HSC, the sinuosity range is 1.5–4.0 (Fig. 3b). As the seafloor slope gradient decreases, the overall downcutting depth decreases (Fig. 3c), so the restricted capacity of the channel is correspondingly weakened. With a decrease in fluid energy, the capacity of the fluid to erode the earlier strata in the channel is insufficient. The fluid bypasses the axial part of the younger channel, and erosion usually occurs on the side of the younger channel with a relatively low sand content. The cross-section shows the lateral accretion or migration trend of the multistage channel, which demonstrates how the sinuosity of the channel is aggravated by this process (Fig. 12b). In addition, according to the seismic cross-sections, the levees of the channel are also relatively well developed at this stage (Figs 10 and 12b), which restricts the lateral movement of the channel to some extent. In such a limited movement space, the channel tends toward equilibrium; thus, the evolution of the channel toward an equilibrium profile is accomplished by the erosion of high-gradient reaches and deposition in the low-gradient portions of the channel (Gee et al., 2007). The width of the channel base is limited within a certain range (150–550 m) (Fig. 3d), so only by changing its sinuosity forms can the channel reach equilibrium.

The MSC has a sinuosity ranging from 1.2 to 1.5 (Fig. 3b), which is between the ranges of the LSC and HSC. In this section, the seafloor slope gradient is the gentlest, and the flow velocity of the fluid is the lowest among the three sections. Hence, after long-distance transport, the energy of the channel fluid is greatly

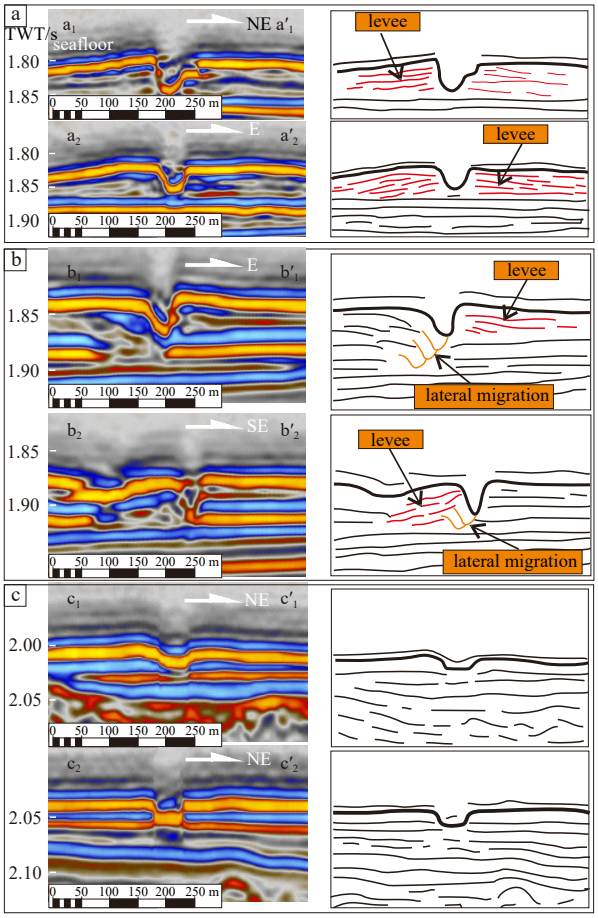

Fig. 12. Seismic cross-sections of the levees in each section of the Channel I. Two seismic cross-sections are selected for each part of the Channel I. a. low-sinuous channel: a_1–a'_1, a_2–a'_2. b. high-sinuous channel: b_1–b'_1, b_2–b'_2. c. moderate-sinuous channel: c_1–c'_1, c_2–c'_2. The seismic cross-sections are on the left, and the interpretation diagrams are on the right. The locations of the seismic cross-sections are shown in Fig. 10.

consumed, and the overall downcutting depth of the channel reaches the minimum value (Fig. 3c). In addition, levees are not well developed in this section (Figs 10 and 12c). Therefore, the limiting effect on the channel basically disappears, the development environment of the channel changes from restricted to nonrestricted, and the lateral movement range of the channel gradually expands. The sinuosity of the original channel gradually increases, and after reaching the maximum value, an abandoned channel is formed through cutoff. However, due to the shallow downcutting depth of the channel, when the fluid laterally erodes the channel wall, it is very easy for a crevasse to form (Fig. 11), resulting in the termination of the lateral erosion of the fluid on the channel sidewall and decreasing the sinuosity of the channel. Therefore, the channel sinuosity in this section is small because frequent crevasses are formed, replacing the changes in the channel sinuosity when the evolution of the channel approaches equilibrium and resulting in the moderately sinuous geometry of this channel section.

6 Conclusions

(1) There are obvious differences in the Channel I morphology on the lower continental slope gradient. According to the quantitative morphological parameters of the Channel I, the Channel I was divided into three types: a LSC, HSC, and MSC. U-shaped channel cross-sections are developed in the LSC, V-shaped channel cross-sections are developed in the HSC, including inclined-V and symmetric-V cross-sections, and dish-shaped channel cross-sections are developed in the MSC.

(2) The sinuosity of a deep-water channel affects its width and depth. A quantitative analysis was performed to explore the interactions between these quantitative parameters, including the width, depth, aspect ratio (width/depth), and sinuosity of each channel section. There were significant differences in the correlations between the quantitative parameters in the different form channel segments. Among them, the LSC has a plane morphology that is not affected by the width or depth, and this channel segment mostly consists of vertical superposition movement. There is a significant negative correlation between the sinuosity and the width of the HSC, which is characterized by lateral movement of the channel. In the MSC, the correlations between the sinuosity and the width and depth of the channel are not significant. This segment is affected by the formation of channel crevasses, and the sinuosity of the channel is moderate.

(3) An interesting phenomenon is observed in the Channel I in this paper: the sinuosity of the middle reaches of the Channel I is much higher than that of the upper and lower reaches. The main factors that cause this phenomenon are the seafloor slope gradient, the differential fluid properties, and the restricted capacity of the channel. The restrictive strength of the Channel I is influenced mainly by the downcutting depth of the channel and the building capacity of the levees. Under the condition of a steep slope, the strong restricted capacity of the Channel I and a large proportion of debris flow in the Channel I, the morphology of the Channel I is relatively straight. However, when the slope is gentle, the limiting ability of the Channel I is weakened. The proportion of turbidity current-induced deposition in the Channel I increases, and the morphology of the Channel I changes accordingly to a sinuous state.

References

Abreu V, Sullivan M, Pirmez C, et al. 2003. Lateral accretion packages (LAPS): an important reservoir element in deep water sinuous channels. Marine and Petroleum Geology, 20(6–8): 631–648

Alpak F O, Barton M D, Naruk S J. 2013. The impact of fine-scale turbidite channel architecture on deep-water reservoir performance. AAPG Bulletin, 97(2): 251–284, doi: 10.1306/04021211067

Babonneau N, Savoye B, Cremer M, et al. 2002. Morphology and architecture of the present canyon and channel system of the Zaire deep-sea fan. Marine and Petroleum Geology, 19(4): 445–467, doi: 10.1016/S0264-8172(02)00009-0

Babonneau N, Savoye B, Cremer M, et al. 2010. Sedimentary architecture in meanders of a submarine channel: Detailed study of the present Congo Turbidite channel (Zaiango Project). Journal of Sedimentary Research, 80(10): 852–866, doi: 10.2110/jsr.2010.078

Biscara L, Mulder T, Martinez P, et al. 2011. Transport of terrestrial organic matter in the Ogooué deep sea turbidite system (Gabon). Marine and Petroleum Geology, 28(5): 1061–1072, doi: 10.1016/j.marpetgeo.2010.12.002

Carter R M, Norris R J. 1976. Cainozoic history of southern New Zealand: an accord between geological observations and plate-tectonic predictions. Earth and Planetary Science Letters, 31(1): 85–94, doi: 10.1016/0012-821X(76)90099-6

Clark J D, Kenyon N H, Pickering K T. 1992. Quantitative analysis of the geometry of submarine channels: implications for the classification of submarine fans. Geology, 20(7): 633–636, doi: 10.1130/0091-7613(1992)020<0633:QAOTGO>2.3.CO;2

Clark J D, Pickering K T. 1996. Architectural elements and growth patterns of submarine channels: application to hydrocarbon ex-

ploration. AAPG Bulletin, 80(2): 194–220
Dai Zhijun, Liu James T, Fu Gui, et al. 2013. A thirteen-year record of bathymetric changes in the North Passage, Changjiang (Yangtze) estuary. Geomorphology, 187: 101–107, doi: 10.1016/j.geomorph.2013.01.004
Dai Zhijun, Mei Xuefei, Darby S E, et al. 2018. Fluvial sediment transfer in the Changjiang (Yangtze) river-estuary depositional system. Journal of Hydrology, 566: 719–734, doi: 10.1016/j.jhydrol.2018.09.019
D'Alpaos A, Ghinassi M, Finotello A, et al. 2017. Tidal meander migration and dynamics: a case study from the Venice Lagoon. Marine and Petroleum Geology, 87: 80–90, doi: 10.1016/j.marpetgeo.2017.04.012
Deptuck M E, Steffens G S, Barton M, et al. 2003. Architecture and evolution of upper fan channel-belts on the Niger Delta slope and in the Arabian Sea. Marine and Petroleum Geology, 20(6–8): 649–676
Deptuck M E, Sylvester Z, Pirmez C, et al. 2007. Migration-aggradation history and 3-D seismic geomorphology of submarine channels in the Pleistocene Benin-major Canyon, western Niger Delta slope. Marine and Petroleum Geology, 24(6–9): 406–433
Dott R H. 1963. Dynamics of subaqueous gravity depositional processes. AAPG Bulletin, 47(1): 104–128
Gabet E J. 1998. Lateral migration and bank erosion in a saltmarsh tidal channel in San Francisco Bay, California. Estuaries, 21(4): 745–753, doi: 10.2307/1353278
Gamboa D, Alves T M. 2015. Spatial and dimensional relationships of submarine slope architectural elements: A seismic-scale analysis from the Espírito Santo Basin (SE Brazil). Marine and Petroleum Geology, 64: 43–57, doi: 10.1016/j.marpetgeo.2015.02.035
Gee M J R, Gawthorpe R L. 2006. Submarine channels controlled by salt tectonics: examples from 3D seismic data offshore Angola. Marine and Petroleum Geology, 23(4): 443–458, doi: 10.1016/j.marpetgeo.2006.01.002
Gee M J R, Gawthorpe R L, Bakke K, et al. 2007. Seismic geomorphology and evolution of submarine channels from the Angolan continental margin. Journal of Sedimentary Research, 77(5): 433–446, doi: 10.2110/jsr.2007.042
Giba M, Walsh J J, Nicol A, et al. 2013. Investigation of the spatio-temporal relationship between normal faulting and arc volcanism on million-year time scales. Journal of the Geological Society, 170(6): 951–962, doi: 10.1144/jgs2012-121
Harishidayat D, Omosanya K O, Johansen S E. 2015. 3D seismic interpretation of the depositional morphology of the middle to late Triassic fluvial system in eastern Hammerfest Basin, Barents Sea. Marine and Petroleum Geology, 68: 470–479, doi: 10.1016/j.marpetgeo.2015.09.007
Higgs K E, Arnot M J, Browne G H, et al. 2010. Reservoir potential of late cretaceous terrestrial to shallow marine sandstones, Taranaki Basin, New Zealand. Marine and Petroleum Geology, 27(9): 1849–1871, doi: 10.1016/j.marpetgeo.2010.08.002
Hudson P F, Kesel R H. 2000. Channel migration and meander-bend curvature in the lower Mississippi River prior to major human modification. Geology, 28(6): 531–534, doi: 10.1130/0091-7613(2000)28<531:CMAMCI>2.0.CO;2
Janocko M, Nemec W, Henriksen S, et al. 2013. The diversity of deep-water sinuous channel belts and slope valley-fill complexes. Marine and Petroleum Geology, 41: 7–34, doi: 10.1016/j.marpetgeo.2012.06.012
Khripounoff A, Vangriesheim A, Babonneau N, et al. 2003. Direct observation of intense turbidity current activity in the Zaire submarine valley at 4000 m water depth. Marine Geology, 194(3–4): 151–158
King P R. 2000. New Zealand's changing configuration in the last 100 million years: plate tectonics, basin development, and depositional setting. In: 2000 New Zealand Petroleum Conference Proceedings. Wellington: Crown Minerals, Ministry of Commerce Wellington, New Zealand
King P R, Thrasher G P. 1996. Cretaceous-Cenozoic geology and petroleum systems of the Taranaki Basin, New Zealand [dissertation]. Lower Hutt: Institute of Geological & Nuclear Sciences
Kolla V. 2007. A review of sinuous channel avulsion patterns in some major deep-sea fans and factors controlling them. Marine and Petroleum Geology, 24(6–9): 450–469
Labourdette R. 2007. Integrated three-dimensional modeling approach of stacked turbidite channels. AAPG Bulletin, 91(11): 1603–1618, doi: 10.1306/06210706143
Li Quan, Wu Wei, Yu Shui, et al. 2017a. The application of three-dimensional seismic spectral decomposition and semblance attribute to characterizing the Deepwater channel depositional elements in the Taranaki Basin of New Zealand. Acta Oceanologica Sinica, 36(9): 79–86, doi: 10.1007/s13131-017-1113-0
Li Lei, Yan Rui, Li Ningtao, et al. 2015. Characteristics and origin of deep-water channels in Rio Muni Basin, West Africa. Geoscience (in Chinese), 29(1): 80–88
Li Quan, Yu Shui, Wu Wei, et al. 2017b. Detection of a deep-water channel in 3D seismic data using the sweetness attribute and seismic geomorphology: a case study from the Taranaki Basin, New Zealand. New Zealand Journal of Geology and Geophysics, 60(3): 199–208, doi: 10.1080/00288306.2017.1307230
Li Lei, Zou Yun, Zhang Peng, et al. 2019. Quantitative analysis of the geometry of sinuous submarine channels: a case from the Rio Muni Basin of Equatorial Guinea. Marine Geology Frontiers (in Chinese), 35(10): 23–35
Liu Xinying, Yu Shui, Hu Xiaolin, et al. 2012. Quantitative relation between the gradient and sinuosity of Deepwater channel and its control: a case study in the Rio Muni Basin, West Africa. Journal of Jilin University (Earth Science Edition) (in Chinese), 42(S1): 127–134
Lowe D R, Graham S A, Malkowski M A, et al. 2019. The role of avulsion and splay development in deep-water channel systems: sedimentology, architecture, and evolution of the deep-water Pliocene Godavari "A" channel complex, India. Marine and Petroleum Geology, 105: 81–99, doi: 10.1016/j.marpetgeo.2019.04.010
Malkowski M A, Jobe Z R, Sharman G R, et al. 2018. Down-slope facies variability within deep-water channel systems: insights from the Upper Cretaceous Cerro Toro Formation, southern Patagonia. Sedimentology, 65(6): 1918–1946, doi: 10.1111/sed.12452
Masalimova L U, Lowe D R, Sharman G R, et al. 2016. Outcrop characterization of a submarine channel-lobe complex: the lower mount messenger formation, Taranaki Basin, New Zealand. Marine and Petroleum Geology, 71: 360–390, doi: 10.1016/j.marpetgeo.2016.01.004
Mayall M, Jones E, Casey M. 2006. Turbidite channel reservoirs-Key elements in facies prediction and effective development. Marine and Petroleum Geology, 23(8): 821–841, doi: 10.1016/j.marpetgeo.2006.08.001
McHargue T, Pyrcz M J, Sullivan M D, et al. 2011. Architecture of turbidite channel systems on the continental slope: patterns and predictions. Marine and Petroleum Geology, 28(3): 728–743, doi: 10.1016/j.marpetgeo.2010.07.008
Mei Xuefei, Dai Zhijun, Wei Wen, et al. 2018. Secular bathymetric variations of the North Channel in the Changjiang (Yangtze) Estuary, China, 1880–2013: causes and effects. Geomorphology, 303: 30–40, doi: 10.1016/j.geomorph.2017.11.014
Mutti E, Normark W R. 1987. Comparing examples of modern and ancient turbidite systems: problems and concepts. In: Leggett J K, Zuffa G G, eds. Marine Clastic Sedimentology. Dordrecht: Springer, 1–38
Niyazi Y, Eruteya O E, Omosanya K O, et al. 2018. Seismic geomorphology of submarine channel-belt complexes in the Pliocene of the Levant Basin, offshore central Israel. Marine Geology, 403: 123–138, doi: 10.1016/j.margeo.2018.05.007
Peakall J, McCaffrey B, Kneller B. 2000. A process model for the evolution, morphology, and architecture of sinuous submarine channels. Journal of Sedimentary Research, 70(3): 434–448, doi: 10.1306/2DC4091C-0E47-11D7-8643000102C1865D
Pichevin L, Bertrand P, Boussafir M, et al. 2004. Organic matter accu-

mulation and preservation controls in a deep sea modern environment: an example from Namibian slope sediments. Organic Geochemistry, 35(5): 543–559, doi: 10.1016/j.orggeochem.2004.01.018

Pirmez C, Imran J. 2003. Reconstruction of turbidity currents in Amazon channel. Marine and Petroleum Geology, 20(6–8): 823–849

Posamentier H W. 2003. Depositional elements associated with a basin floor channel-levee system: case study from the Gulf of Mexico. Marine and Petroleum Geology, 20(6–8): 677–690

Qin Yongpeng, Alves T M, Constantine J, et al. 2016. Quantitative seismic geomorphology of a submarine channel system in SE Brazil (Espírito Santo Basin): scale comparison with other submarine channel systems. Marine and Petroleum Geology, 78: 455–473, doi: 10.1016/j.marpetgeo.2016.09.024

Reimchen A P, Hubbard S M, Stright L, et al. 2016. Using sea-floor morphometrics to constrain stratigraphic models of sinuous submarine channel systems. Marine and Petroleum Geology, 77: 92–115, doi: 10.1016/j.marpetgeo.2016.06.003

Rotzien J R. 2013. Processes of sedimentation, stratigraphic architecture, and provenance of deep-water depositional systems: the upper Miocene Upper Mount messenger formation, Taranaki Basin, New Zealand and Pliocene Repetto and Pico formations, Ventura Basin, California [dissertation]. Stanford: Stanford University, 218

Rotzien J R, Lowe D R, King P R, et al. 2014. Stratigraphic architecture and evolution of a deep-water slope channel-levee and overbank apron: the Upper Miocene Upper Mount Messenger Formation, Taranaki Basin. Marine and Petroleum Geology, 52: 22–41, doi: 10.1016/j.marpetgeo.2014.01.006

Stagpoole V M, Hill M, Thornton S, et al. 2002. New Zealand Basin development and depositional systems evolution: quantification and Visualisation. In: 2002 New Zealand Petroleum Conference Proceedings. Auckland: GNS Science, 351–362

Straub K M, Mohrig D, Buttles J, et al. 2011. Quantifying the influence of channel sinuosity on the depositional mechanics of channelized turbidity currents: a laboratory study. Marine and Petroleum Geology, 28(3): 744–760, doi: 10.1016/j.marpetgeo.2010.05.014

Sutherland R. 1999. Basement geology and tectonic development of the greater New Zealand region: an interpretation from regional magnetic data. Tectonophysics, 308(3): 341–362, doi: 10.1016/S0040-1951(99)00108-0

Tek D E, McArthur A D, Poyatos-Moré M, et al. 2022. Controls on the architectural evolution of deep-water channel overbank sediment wave fields: insights from the Hikurangi Channel, offshore New Zealand. New Zealand Journal of Geology and Geophysics, 65(1): 141–178, doi: 10.1080/00288306.2021.1978509

Uruski C I. 2008. Deepwater Taranaki, New Zealand: structural development and petroleum potential. Exploration Geophysics, 39(2): 94–107, doi: 10.1071/EG08013

Uruski C I. 2010. New Zealand's Deepwater frontier. Marine and Petroleum Geology, 27(9): 2005–2026, doi: 10.1016/j.marpetgeo.2010.05.010

Wynn R B, Cronin B T, Peakall J. 2007. Sinuous deep-water channels: Genesis, geometry and architecture. Marine and Petroleum Geology, 24(6–9): 341–387

Xu Jie, Snedden J W, Galloway W E, et al. 2017. Channel-belt scaling relationship and application to early Miocene source-to-sink systems in the Gulf of Mexico Basin. Geosphere, 13(1): 179–200, doi: 10.1130/GES01376.1

Yao Yue, Zhou Jiangyu, Lei Zhenyu, et al. 2018. High restriction seismic facies and inner structural segmentation features of the central canyon channel systems in Xisha trough basin. Acta Sedimentologica Sinica (in Chinese), 36(4): 787–795

Zhao Xiaoming, Liu Li, Tan Chengpeng, et al. 2018a. Styles of submarine-channel architecture and its controlling factors: a case study from the Niger Delta Basin slope. Journal of Palaeogeography (in Chinese), 20(5): 825–840

Zhao Xiaoming, Qi Kun, Liu Li, et al. 2018b. Development of a partially-avulsed submarine channel on the Niger Delta continental slope: architecture and controlling factors. Marine and Petroleum Geology, 95: 30–49, doi: 10.1016/j.marpetgeo.2018.04.015

Zhou Xiaoyan, Dai Zhijun, Mei Xuefei. 2020. The multi-decadal morphodynamic changes of the mouth bar in a mixed fluvial-tidal estuarine channel. Marine Geology, 429: 106311, doi: 10.1016/j.margeo.2020.106311

Zucker E, Gvirtzman Z, Steinberg J, et al. 2017. Diversion and morphology of submarine channels in response to regional slopes and localized salt tectonics, Levant Basin. Marine and Petroleum Geology, 81: 98–111, doi: 10.1016/j.marpetgeo.2017.01.002